Composites Part B 98 (2016) 70–77

Contents lists available at ScienceDirect

Composites Part B

journal homepage: www.elsevier.com/locate/compositesb

Mechanical behavior of polylactic acid/polycaprolactone porous layered functional composites

Roberto Scaffaro*, Francesco Lopresti, Luigi Botta, Andrea Maio

University of Palermo, Dipartimento di Ingegneria Civile, Ambientale, Aerospaziale, dei Materiali, UdR INSTM di Palermo, Viale delle Scienze Ed. 6, 90128 Palermo, Italy

ARTICLE INFO

Article history:
Received 14 December 2015
Received in revised form
4 April 2016
Accepted 9 May 2016
Available online 12 May 2016

Keywords:
Layered structures
Adhesion
Mechanical properties
Compression molding
Functionally graded materials

ABSTRACT

Biopolymeric porous devices exhibiting graded properties can play a crucial role in several fields, such as tissue engineering or controlled drugs release. In this context, the gradient of a specific property can be achieved by developing porous laminates composed by different types of materials. This work presents for the first time a multi-phasic porous laminate based on polycaprolactone (PCL) and polylactic acid (PLA) prepared by combining melt mixing, compression molding and particle leaching. All the materials were characterized from a morphological and a mechanical point of view.

The results put into evidence the possibility to tune and to predict the mechanical properties by controlling the process parameters together with geometrical features.

1. Introduction

Over the past decades there has been a growing interest toward polymeric materials obtained by renewable sources and with potential biodegradability or compostability to reduce the overall environmental impact [1–10].

In particular, porous biopolymeric devices with engineered chemical, physical and mechanical properties can play a crucial role in biomedical fields, such as tissue engineering or controlled drugs release [11–14].

The development of porous laminates composed by different kinds of biopolymer allow controlling these parameters by tuning the properties of each single layer and by eventually assembling them into a single device [15–17]. This feature is of main concern for interface tissue engineering (ITE), a rapidly developing field that aims to the production of structures designed either to repair or to regenerate diseased or damaged zones at the interface of different types of tissue. Interface tissues are more complex than the homogeneous ones because of the presence of multi-phasic and/or anisotropic structures that gradually change from one tissue to another [11,16,17]. The desire to mimic these natural structures has driven biomechanical engineers to develop custom-made bio-inspired materials with mechanical properties similar to natural tissues [15,18,19]. Usually, porous multiphasic laminates are developed by 3D printing, suturing, glue or press fitting two/three layers, even if the best challenge is achieving a well joint monolith presenting functionally graded properties [17,20–28].

In this context, synthetic biodegradable polymers used in tissue engineering or in other biomedical applications include polylactic acid (PLA) and polycaprolactone (PCL).

PCL is a semicrystalline thermoplastic polymer with low melt temperature, thus enabling the possibility to be easily melt processed [29]. Hydrolytically labile ester linkages are responsible for its degradation although slow (2–3 years) [30]. In addition, it is a ductile polymer at room temperature, with a relative low elastic modulus [31,32].

PLA melting point is higher if compared with that of PCL, although it presents a fragile behavior with high elastic modulus and low elongation at break. For this reason, this latter is preferred for bone repair, whereas the former is usually chosen for the cartilage regeneration [33,34].

In this work, we developed for the first time a chemically graded laminate porous device composed by a PLA-based core and a PCL-based shell in form of monolith.

The novelty of this work can be principally ascribed to the preparation route of the multiphasic porous laminates, conducted

* Corresponding author.
E-mail address: roberto.scaffaro@unipa.it (R. Scaffaro).

http://dx.doi.org/10.1016/j.compositesb.2016.05.023
1359-8368/

by melt. In fact, the devices were fabricated by combining melt mixing, compression molding and particulate leaching. The principal advantages of this method lay in the absence of organic solvents during the preparation and in the possibility to easily control and predict both porosity (void-to-total volume ratio) and pore size, by tuning the amount and the dimension of porogen particles, respectively.

The relative volume ratio was controlled by the thickness of each layer in order to investigate the correlation between the preparation, the morphology and mechanical properties of three-layered laminate based on PCL and PLA. In particular, the study of mechanical properties of porous bio-laminates were investigated as a function of the relative contribution of the layers to the whole laminated device.

2. Materials and methods

The PLA used in the frame of this work was a sample purchased by Natureworks (PLA 2002D, density 1.24 g/cm^3) while poly(-ethylene glycol) (PEG), Mw = 2000 Da, and PCL, Mw = 80,000 Da, were purchased by Sigma Aldrich, as well as NaCl (purity > 99%, d = 2.17 g/cm^3). Little amounts (less than 1%) of green PLA filament (Matter Hackers, USA) was used as a masterbatch in order to stain and distinguish the PLA phase from PCL.

In order to avoid hydrolytic scission during processing, all the materials were vacuum dried overnight [35]. More in detail, for each polymer the drying temperature was kept below its own glass transition temperature: i.e. 90 °C for PLA, 25 °C for PEG and 40 °C for PCL. NaCl was dried at 105 °C to ensure the highest drying degree.

The NaCl was sieved in the range of 90–110 μm to obtain homogeneous pore size distribution.

2.1. Laminates fabrication

Porous laminates were prepared by melt mixing as described in our previous works [12,13]. In brief, PLA (or PCL), PEG and NaCl, with weight percentage composition of respectively 20/5/75, were fed to a batch mixer (Plasticorder PLE-330 Brabender, Germany). The temperature was set to 190 °C in the case of PLA and to 100 °C for PCL, the rotor speed was 64 rpm, the mixing time was around 10 min, in order to ensure achieving a constant value of torque. Thereafter, the samples were fed out and rapidly cooled in liquid nitrogen. The materials collected were ground and compression-molded in a laboratory press (Carver, USA) at 190 °C for PLA and 100 °C for PCL at 180 bar in appropriate cylindrical molds with a diameter of 10 mm and different thickness as summarized in Table 1. The pre-compressed monolayers were finally assembled by further compression molding at 130 °C at 180 bar, in order to obtain the final laminates.

Finally, the porogen part of the blends (NaCl and PEG) was removed by selective leaching in demineralized water for 5 h. The resulting structure were then allowed to dry for 12 h at room temperature. Laminates are schematically represented in Fig. 1.

Table 1
Sample code of the mono-phasic and multi-phasic porous laminates as a function of the thickness of each layer.

Sample code	PCL Layer (mm)	PLA Layer (mm)	PCL Layer (mm)
PCL	3	0	0
LAM_0.5	1.25	0.5	1.25
LAM_1	1	1	1
LAM_2	0.5	2	0.5
PLA	0	3	0

2.2. Morphological analysis

The morphology of the laminates was evaluated by scanning electron microscopy (SEM), by using a Phenom Pro x, Phenom-World (The Netherlands). The samples, cryo-fractured in liquid nitrogen, were attached on an aluminum stub using an adhesive carbon tape and then sputter coated with gold (Sputtering Scancoat Six, Edwards, UK) for 90 s under argon atmosphere before imaging to avoid electrostatic discharge under the electron beam.

2.3. Laminate pore size

Pore size analysis was carried out using a MATLAB (MathWorks Inc., MA, USA)-based software previously described [36]. The custom-made software is able to accomplish the segmentation of images containing pores of any geometry in a semi-automatic way, and it converts the digital images into binary form, thus calculating the pores area distribution (PAD); the software reports the percentage of the total area occupied by the pores having diameters in a given interval. The red, green and blue colors are assigned to three increasing intervals of the size of the pores.

2.4. Porosity, connectivity, water uptake

The parameters related to porous properties of the laminate were obtained by gravimetric measurement. Theoretical porosity, porosity and connectivity were calculated according to the following expressions [37]:

$$Porosity_{th}(\%) = \frac{V_{porogen}}{V_{total}} \times 100\% \quad (1)$$

$$Porosity(\%) = \left(1 - \frac{\rho_{laminate}}{\rho_{matrix}}\right) \times 100 \quad (2)$$

$$Connectivity = \frac{\left(m_0 - m_{dry}\right)}{m_{NaCl} + m_{PEG}} \times 100\% \quad (3)$$

Where, m_{NaCl}, m_{PEG} are the theoretical weights of NaCl and PEG, respectively, by assuming a homogeneous mixture. m_0 and m_{dry} are, respectively, the weights of laminate before leaching and after leaching and drying. The density (ρ) of NaCl, PEG, PLA and PCL are respectively 2.16 g/cm^3, 1.12 g/cm^3 and 1.24 g/cm^3 and 1.14 g/cm^3. $\rho_{laminate}$ is the apparent density of the laminate.

The theoretical porosity was calculated by assuming the complete solvation of all the porogen agents (PEG plus NaCl). The real porosity was calculated as the reciprocal of the ratio between the apparent densities of the laminate and of the non-porous polymeric material, by using expression (2). It expresses the ratio between the empty volume and the overall volume of the laminate (empty + full). The connectivity is a parameter indicating the continuity of the porogen phases and was assessed by using Eq. (3), i.e. by taking into account the weight variation of the laminate before and after the porogen agent extraction, with respect to the overall weight of porogen compounds.

The bulk water absorption (water uptake) was calculated as the difference between the weight of the devices filled by water (m_{wet}) and the weight after drying in fume hood, according to Eq. (4):

$$Water\ uptake(\%) = \left(\frac{m_{wet} - m_{dry}}{m_{dry}}\right) \times 100\% \quad (4)$$

The percentage of pores filled by water was evaluated as the

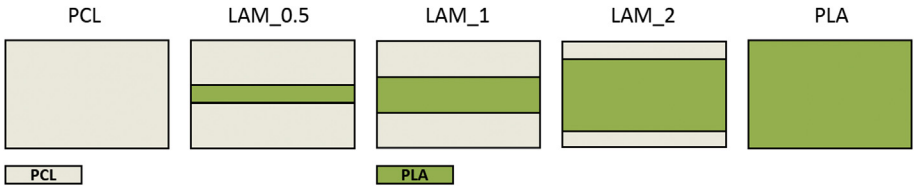

Fig. 1. Schematic representation of the laminates design.

ratio between the volume of water into the laminate and the empty volume, given by the real porosity. The volume of water filled by the devices was measured as the weight difference between the dry and wet sample. For these measurements a precision balance with a resolution of ±0.1 mg was used (Sartorius AX224, Germany).

2.5. Mechanical properties

The scaffolds were mechanically tested in compression using an Instron 3365 (UK) with BioPuls Bath (Norwood, MA). The tests were performed both in PBS, (pH = 7.4) at 37 °C (wet condition) and in air at room temperature (dry condition). Samples were prepared to measurements in BioPuls Bath, filling them with PBS in a vacuum flask for 5 min to let PBS to fill all the pores. Subsequently scaffolds were left in PBS at 37 °C for 15 min to achieve the testing temperature. The 10 mm × 3 mm (3:10 height to diameter ratio) scaffolds were tested in compression until failure with a uniform strain rate of 1 mm min^{-1} with a 1 kN load cell. The data were analyzed to determine elastic modulus. The tensile stress-strain curves were determined by means of a custom-designed interfacial strength test equipment fitted to the Instron 3365 (UK) apparatus, following a method described in the scientific literature [13,21]. The rig design allows the secure fixation of the specimen during testing and ensures its correct alignment between load cell and base platen. Scaffold samples were adhered to aluminum test stubs using a high viscosity adhesive (Patter Power Epoxy) and inserted into the equipment for testing. A 1 kN load cell was used under a tensile load applied at a strain rate of 1 mm min^{-1}. Failure was expected to occur either at the ultimate tensile strength of one of the component layers of the scaffold or because of delamination at the layer interfaces. Interfacial adhesion strength was measured as the maximum strength of the stress strain curve.

3. Results

3.1. Morphological analysis

Fig. 2a–f show SEM micrographs of monolayer and multi-phasic laminates.

In particular, Fig. 2a refers to the device containing only PCL, characterized by a homogenous pores size distribution. Fig 2b shows the laminate LAM_0.5 characterized by a PLA-based core layer (500 μm thick), evidenced by the red lines and a PCL-based shell. Fig. 2c reports the laminate developed by assembling 1 mm of PCL (top), 1 mm of PLA (core) and 1 mm of PCL (bottom) (LAM_1). Fig. 2d shows the morphology of the LAM_2, the multilayer with the highest volumetric fraction of PLA, while Fig. 2e shows the device composed entirely of PLA.

These pictures suggest that the macro-pore architecture (about 100 μm) of the laminates is not dependent on the kind of material but only on the granulometry of the sieved NaCl filled during the melt mixing process, that was in the range of 90–110 μm. Indeed, the morphology of the multi-phasic laminates, reported in Fig. 2b,c, is very similar to those of the monophasic devices (Fig. 2a,e), as further confirmed by the pore area distribution (PAD) calculated by image processing and reported in Fig 3a–c. The histograms put into evidence that all the laminates present a similar PAD with a concentration of pores within the range 90–110 μm, the same as the sieved salt particles, thus confirming that the macropores network can be controlled, tuned and predicted by the granulometry of the salt filled in the polymer matrix.

Moreover, by comparing the morphologies of PCL (Fig. 3a) and PLA (Fig. 3c), it is possible to detect a higher amount of pores around 10 μm for PCL sample.

In fact, SEM analysis carried out at higher magnification showed that the two phases exhibit slight differences in the pores architecture. Fig. 4a,b reports the micrographs taken at the interface region between the PCL (top) and the PLA (bottom) layer of the

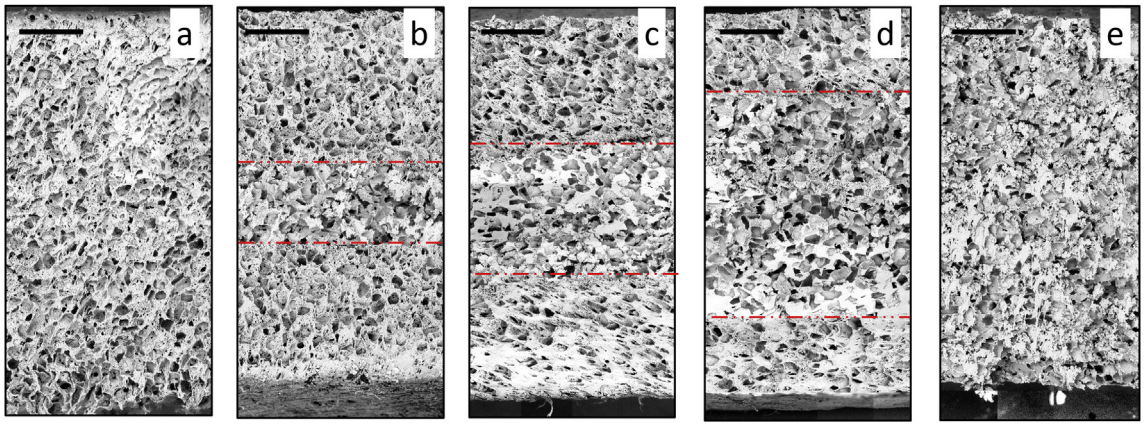

Fig. 2. SEM images of porous laminates: a) PCL sample; b) PCL laminate with PLA core 0.5 mm thick (LAM_0.5); c) PCL laminate with PLA core 1 mm thick (LAM_1); d) PCL laminate with PLA core 2 mm thick (LAM_2) and e) PLA sample. Scale bar is 500 μm.

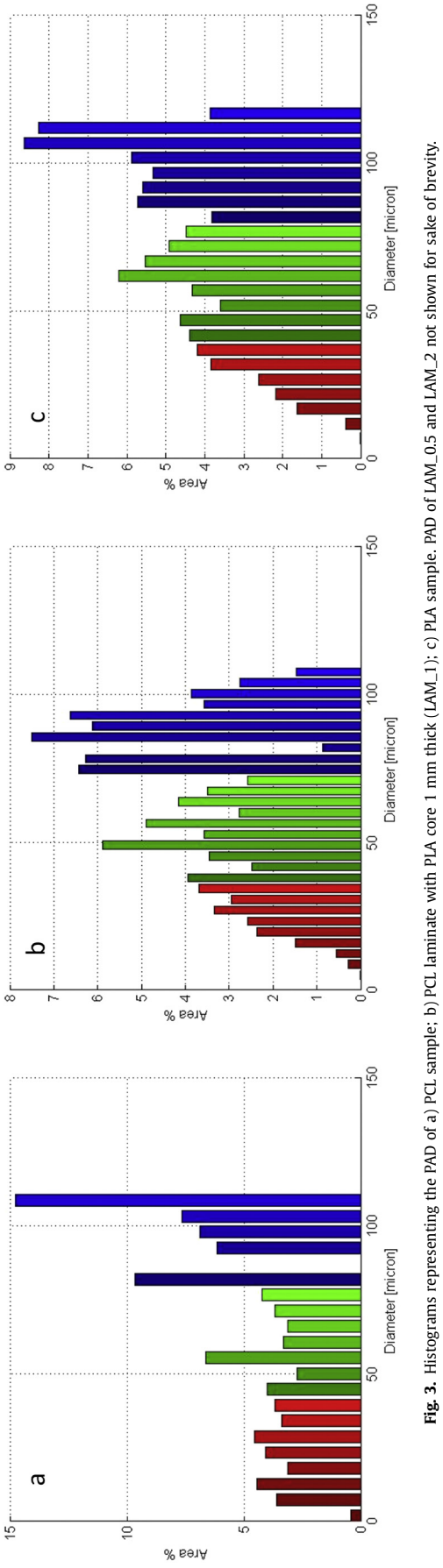

Fig. 3. Histograms representing the PAD of a) PCL sample; b) PCL laminate with PLA core 1 mm thick (LAM_1); c) PLA sample. PAD of LAM_0.5 and LAM_2 not shown for sake of brevity.

LAM_1, chosen as representative multi-phasic laminate for sake of brevity. Fig. 4a confirms that the macropore structure of the two layers is very similar but the PCL phase is characterized by a continuous network of micro-pores (about 5 μm), likely due to the solvation of the PEG phase [12], clearly visible at higher magnification (see Fig. 4b). Even the PLA region presents a microporous network due to the PEG solvation [13] but, owing to the higher solubility of PEG in PLA, the concentration of micro-pores is significantly lower than those observed within PCL layers. Moreover, PAD analysis carried out by image processing strongly confirm this hypothesis. (Fig. 3c).

The presence of the microporous network in the PCL phase allowed us to better distinguish each layer during SEM observations; however, one of the polymeric phases (PLA) was colored with a green pigment in order to better identify each polymer, thus providing further confirmation that each relative layer thickness was effectively developed according to the previous design. Fig. 5a–c show the digital pictures of LAM_0.5, LAM_1 and LAM_2 sections. The images confirmed that the method here presented allowed achieving the full control of the thickness for each layer composing the laminate. In fact, the whole sample is 3 mm high in all the cases, the thickness of green stained PLA layer is about equal to 500 μm (Fig. 5a), 1000 μm (Fig. 5b) and 2000 μm (Fig. 5c), in compliance with the planned design.

Another important morphological analysis regarded the interface between each layer of the composite. In Fig. 2b–d it can be observed that the entire device does not present any internal cleavages; moreover, no discontinuity can be distinguished in the interlayer region. The high adhesion is clearly visible even in Fig. 4a,b and further confirmed by tensile tests, as will be better discussed below.

3.2. Porosity, connectivity and water uptake analysis

Table 2 summarizes theoretical porosity (%), porosity (%), connectivity (%) and water uptake (%) for each different laminate. In this work, the formulation of the mixture was designed in order to obtain scaffolds with a theoretical porosity of 70.8%. The porosity, calculated by Eq. (2), is very close to that theoretically predicted for all the laminates, hence suggesting that all the porogen agents were extracted from devices within the leaching step [12,13]. The data collected about the connectivity, calculated according to Eq. (3) and resulted higher than 99% for all the samples, strongly confirm this hypothesis. The laminates showed a water uptake ranging within 220% (for neat PCL) and 290% (for neat PLA) likely due to the different wettability of the polymers. Consequently, the multiphasic samples displayed a water uptake dependent on the content of PLA. The higher the PLA amount the higher the water uptake.

3.3. Laminates tensile mechanical behavior

Fig. 6 reports the experimental and theoretical (iso-stress model prediction) data carried out from tensile tests. In particular, Young's modulus, reported in Fig. 6a, was found to strongly depend on the relative thickness of the different layers, i.e. the larger the PLA layer the higher the E value. Furthermore, the iso-stress model, which is valid if each layer of the composite is ideally subjected at the same stress, fits very well the experimental data collected; that is reasonably due to the high adhesion strength between the different layers of the laminates.

The high adhesion strength is confirmed by the maximum stress values plotted in Fig. 6b. Tensile strength is 1.6 MPa for the porous PCL and 360 kPa for PLA. The multi-phasic laminates showed a tensile strength comparable with the PLA laminate and

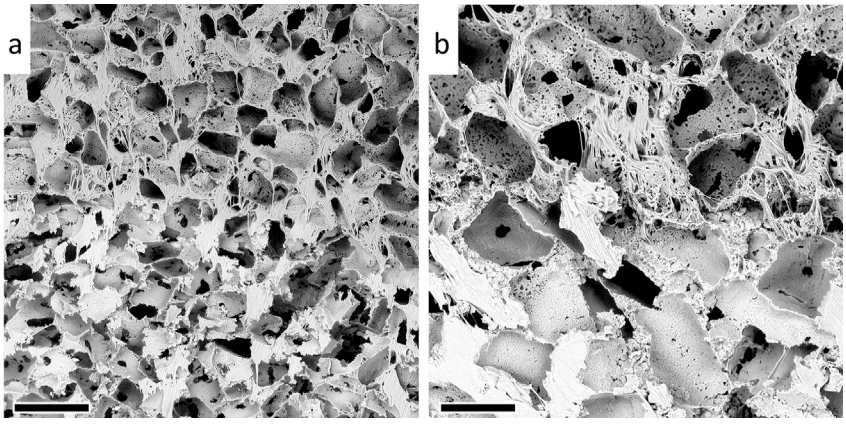

Fig. 4. SEM images of the interface region between the PCL (top) and PLA (bottom) layer of the sample C. a) Scale bar is 200 μm b) Scale bar is 100 μm.

Fig. 5. Digital photo of sections of the multi-phasic laminates with the PLA core layer green colored. a) PCL laminate with PLA core 0.5 mm thick (LAM_0.5); b) PCL laminate with PLA core 1 mm thick (LAM_1); c) PCL laminate with PLA core 2 mm thick (LAM_2). Scale bar is 1 mm. (For interpretation of the references to colour in this figure legend, the reader is referred to the web version of this article.)

Table 2
Theoretical porosity (%), porosity (%), connectivity (%), water uptake (%) as a function of the type of laminate.

Sample code	Theoretical porosity (%)	Porosity (%)	Connectivity (%)	Water uptake (%)
PCL	70.84	70.18 ± 0.55	99.45 ± 0.15	220.2 ± 11.4
LAM_0.5	70.84	69.84 ± 0.42	99.32 ± 0.14	270.3 ± 14.7
LAM_1	70.84	69.97 ± 0.47	99.54 ± 0.22	280.8 ± 7.1
LAM_2	70.84	69.55 ± 0.72	99.60 ± 0.20	285.5 ± 13.3
PLA	70.84	70.25 ± 0.42	99.50 ± 0.22	290.5 ± 10.2

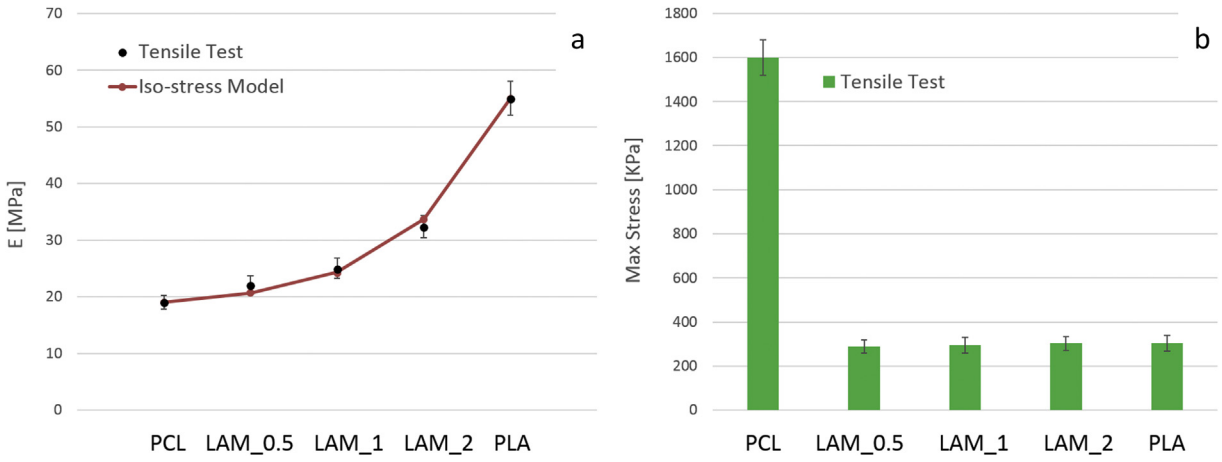

Fig. 6. a) E modulus and iso-stress model of the tensile mechanical test for the different laminates; b) Tensile stress for the different laminates.

the fracture always occurred in the PLA region, as highlighted in Fig. 7a–d, and never at the interface. This feature demonstrates that the adhesion strength is higher than the ultimate resistance of the PLA layer.

In order to ensure that the fracture of the device occurred in the PLA layer, ATR analysis were carried out on both the fracture surfaces. The spectra, reported in Fig. 8a,b, show the typical peaks of the PLA, as listed in Table 3, thus ensuring that the fracture occurred within the PLA layer for all the multi-phasic laminates investigated [38].

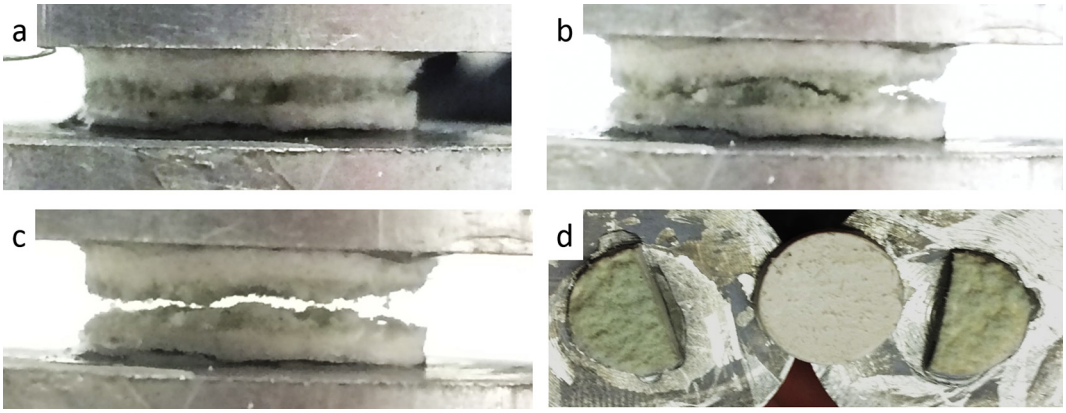

Fig. 7. Digital photo of the LAM_1 tensile test at different deformation. a) not deformed; b) the crack start in the PLA layer (green); c) complete fracture; d) surface fracture of the sample is green, the white laminate in the center is to see better the color contrast. (For interpretation of the references to colour in this figure legend, the reader is referred to the web version of this article.)

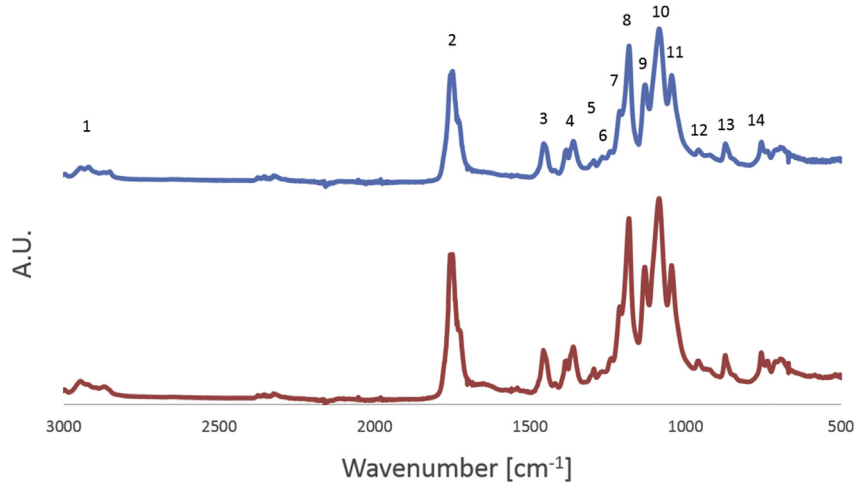

Fig. 8. ATR-FTIR of both the fractured surfaces of the LAM_1 sample. It presents the typical peaks of the PLA for both the fractured surfaces.

Table 3
Peak band assignment for PLA [38].

Peak number	Assignment	Wavenumber cm^{-1}
1	–CH- stretch	3000 (*asym.*),
2	–C═O carbonyl stretch	2948 (*sym.*),
3	$-CH_3$ bending	1747
4	–CH- asymmetric; symmetric deformation	1456
5	–CH- bending	1382; 1360
6	–C–O- stretching	1315–1300
7	–C═O bending	1265
8,9,10	–C–O- stretching	1211
11	–OH bending	1180, 1129, 1083
12	$-CH_3$ rocking mode	955, 916
13	–C–C- stretching crystalline phase	869
14	Amorphous phase	755

3.4. Laminates compressive mechanical behavior

Fig. 9a,b reports the mechanical behavior under compression and the corresponding iso-stress model predictions for all the samples. The elastic modulus (Fig. 9a), in this case, was practically constant and equal to about 7 MPa.

Getting into the details, one may notice that the compressive modulus was found to depend only on the weakest layer (PCL), regardless of PLA thickness [12,13]. For this reason, the iso-stress model was unable to predict the experimental data (Fig. 9a).

These results can be likely explained by considering that the aspect ratio of the cell ribs, characterized by a very low thickness in comparison with their height (i.e. pore diameter), makes them prone to elastic buckling [25]. This phenomenon, occurring only under compression, mainly affects the softest layer. Likely due to this feature, the experimental data for the multi-phasic structures remain practically constant and close to that of PCL.

In the last region of the stress-strain curves, σ was found to

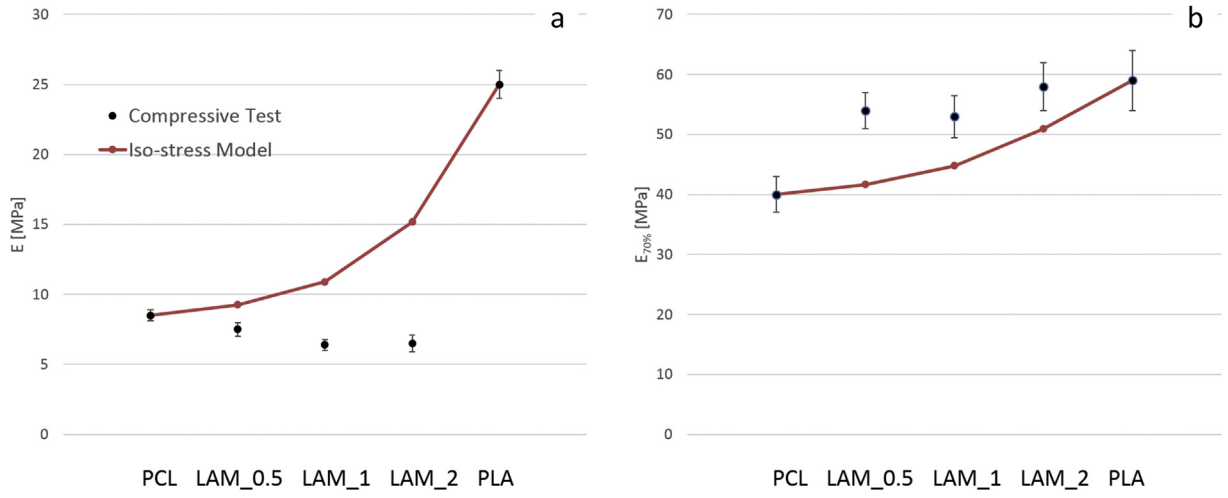

Fig. 9. a) E modulus and iso-stress model of the compressive mechanical test for the different laminates; b) E_D measured in the linear densification region and iso-stress prediction.

linearly increase as a function of the strain. This feature can be ascribed to the densification phenomena occurring since the pore walls collapsed thus filling the voids. The slope of this linear zone (E_D) was then measured and plotted in Fig. 9b as a function of the PLA thickness.

Except for the PCL, this property levels off, remaining equal to that of PLA, i.e. around 55 MPa. Even in this case, the iso-stress model is unable to fit the experimental data. Interestingly, E_D seems to be totally controlled by the PLA layer.

4. Conclusions

In this work, porous PCL/PLA multi-phasic laminates were prepared by combining melt mixing, compression molding and selective leaching. The devices showed highly interconnected porous structure with a porosity of 70%. This eco-friendly technique ensures achieving high predictability of both pore size and porosity, by simply tuning the amount and the granulometry of NaCl, respectively as confirmed by SEM, image processing and gravimetric analyses.

Morphological and mechanical analyses highlighted that three-layered laminates are characterized by well joint regions without loss of adhesion or interface fracture.

Tensile mechanical tests showed the strong correlation between E value and the relative thickness of the layers composing the laminates, with a trend that strongly follows the iso-stress model predictions. Compressive mechanical tests showed that the E value is controlled by the weakest layer composing the multi-phasic laminates i.e. the PCL.

In conclusion, this approach permits to design multi-phasic porous devices with a high control of both morphological and mechanical characteristics.

References

[1] Fiore V, Botta L, Scaffaro R, Valenza A, Pirrotta A. PLA based biocomposites reinforced with Arundo donax fillers. Compos Sci Technol 2014;105:110–7. http://dx.doi.org/10.1016/j.compscitech.2014.10.005.

[2] Scaffaro R, Botta L, Sanfilippo M, Gallo G, Palazzolo G, Puglia AM. Combining in the melt physical and biological properties of poly(caprolactone) and chlorhexidine to obtain antimicrobial surgical monofilaments. Appl Microbiol Biotechnol 2013;97:99–109. http://dx.doi.org/10.1007/s00253-012-4283-x.

[3] Scaffaro R, Botta L, Passaglia E, Oberhauser W, Frediani M, Di Landro L. Comparison of different processing methods to prepare poly(lactid acid)-hydrotalcite composites. Polym Eng Sci 2014;54:1804–10. http://dx.doi.org/10.1002/pen.23724.

[4] Scaffaro R, Botta L, Gallo G, Puglia AM. Influence of drawing on the antimicrobial and physical properties of chlorhexidine-compounded poly(-caprolactone) monofilaments. Macromol Mater Eng 2015;12:1268–77. http://dx.doi.org/10.1002/mame.201500121.

[5] Ho M, Lau K, Wang H, Hui D. Improvement on the properties of polylactic acid (PLA) using bamboo charcoal particles. Compos Part B Eng 2015;81:14–25. http://dx.doi.org/10.1016/j.compositesb.2015.05.048.

[6] Morreale M, Scaffaro R, Maio A, La Mantia FP. Mechanical behaviour of Mater-Bi/wood flour composites: a statistical approach. Compos Part A Appl Sci Manuf 2008;39:1537–46. http://dx.doi.org/10.1016/j.compositesa.2008.05.015.

[7] Arrieta MP, Fortunati E, Dominici F, Rayón E, López J, Kenny JM. PLA-PHB/cellulose based films: mechanical, barrier and disintegration properties. Polym Degrad Stab 2014;107:139–49. http://dx.doi.org/10.1016/j.polymdegradstab.2014.05.010.

[8] Siqueira G, Bras J, Dufresne A. New process of chemical grafting of cellulose nanoparticles with a long chain isocyanate. Langmuir 2010;26:402–11. http://dx.doi.org/10.1021/la9028595.

[9] Song Z, Xiao H, Zhao Y. Hydrophobic-modified nano-cellulose fiber/PLA biodegradable composites for lowering water vapor transmission rate (WVTR) of paper. Carbohydr Polym 2014;111:442–8. http://dx.doi.org/10.1016/j.carbpol.2014.04.049.

[10] Zhou C, Shi Q, Guo W, Terrell L, Qureshi AT, Hayes DJ, et al. Electrospun bio-nanocomposite scaffolds for bone tissue engineering by cellulose nanocrystals reinforcing maleic anhydride grafted PLA. ACS Appl Mater Interfaces 2013;5:3847–54. http://dx.doi.org/10.1021/am4005072.

[11] Seidi A, Ramalingam M, Elloumi-Hannachi I, Ostrovidov S, Khademhosseini A. Gradient biomaterials for soft-to-hard interface tissue engineering. Acta Biomater 2011;7:1441–51. http://dx.doi.org/10.1016/j.actbio.2011.01.011.

[12] Scaffaro R, Lopresti F, Botta L, Rigogliuso S, Ghersi G. Melt processed PCL/PEG scaffold with discrete pore size gradient for selective cellular infiltration. Macromol Mater Eng 2016;301:182–90. http://dx.doi.org/10.1002/mame.201500289.

[13] Scaffaro R, Lopresti F, Botta L, Rigogliuso S, Ghersi G. Preparation of three-layered porous PLA/PEG scaffold: relationship between morphology, mechanical behavior and cell permeability. J Mech Behav Biomed Mater 2016;54:8–20. http://dx.doi.org/10.1016/j.jmbbm.2015.08.033.

[14] Murphy CM, Haugh MG, O'Brien FJ. The effect of mean pore size on cell attachment, proliferation and migration in collagen-glycosaminoglycan scaffolds for bone tissue engineering. Biomaterials 2010;31:461–6. http://dx.doi.org/10.1016/j.biomaterials.2009.09.063.

[15] Mi H-Y, Jing X, Yu E, McNulty J, Peng X-F, Turng L-S. Fabrication of triple-layered vascular scaffolds by combining electrospinning, braiding, and thermally induced phase separation. Mater Lett 2015;161:305–8.

[16] Jelen C, Mattei G, Montemurro F, De Maria C, Mattioli-Belmonte M, Vozzi G. Bone scaffolds with homogeneous and discrete gradient mechanical properties. Mater Sci Eng C Mater Biol Appl 2013;33:28–36. http://dx.doi.org/10.1016/j.msec.2012.07.046.

[17] Yousefi A-M, Hoque ME, Prasad RGSV, Uth N. Current strategies in multiphasic scaffold design for osteochondral tissue engineering: a review. J Biomed Mater Res Part A 2015;103:2460–81. http://dx.doi.org/10.1002/jbm.a.35356.

[18] Yusong P, Qianqian S, Chengling P, Jing W. Prediction of mechanical properties of multilayer gradient hydroxyapatite reinforced poly(vinyl alcohol) gel biomaterial. J Biomed Mater Res Part B Appl Biomater 2013;101 B:729–35. http://dx.doi.org/10.1002/jbm.b.32875.

[19] Bai H, Wang D, Delattre B, Gao W, De Coninck J, Li S, et al. Biomimetic gradient scaffold from ice-templating for self-seeding of cells with capillary effect. Acta

Biomater 2015;20:113–9. http://dx.doi.org/10.1016/j.actbio.2015.04.007.
[20] Harley BA, Lynn AK, Wissner-Gross Z, Bonfield W, Yannas IV, Gibson LJ. Design of a multiphase osteochondral scaffold. II. Fabrication of a mineralized collagen–glycosaminoglycan scaffold. J Biomed Mater Res Part A 2010;92:1066–77.
[21] Levingstone TJ, Matsiko A, Dickson GR, O'Brien FJ, Gleeson JP. A biomimetic multi-layered collagen-based scaffold for osteochondral repair. Acta Biomater 2014;10:1996–2004. http://dx.doi.org/10.1016/j.actbio.2014.01.005.
[22] Swieszkowski W, Tuan BHS, Kurzydlowski KJ, Hutmacher DW. Repair and regeneration of osteochondral defects in the articular joints. Biomol Eng 2007;24:489–95.
[23] Fedorovich NE, Schuurman W, Wijnberg HM, Prins H-J, van Weeren PR, Malda J, et al. Biofabrication of osteochondral tissue equivalents by printing topologically defined, cell-laden hydrogel scaffolds. Tissue Eng Part C Methods 2011;18:33–44. http://dx.doi.org/10.1089/ten.TEC.2011.0060.
[24] Laurent CP, Durville D, Mainard D, Ganghoffer JF, Rahouadj R. A multilayer braided scaffold for anterior cruciate ligament: mechanical modeling at the fiber scale. J Mech Behav Biomed Mater 2012;12:184–96. http://dx.doi.org/10.1016/j.jmbbm.2012.03.005.
[25] Lee M, Wu BM. Recent advances in 3D printing of tissue engineering scaffolds. Methods Mol Biol 2012;868:257–67. http://dx.doi.org/10.1007/978-1-61779-764-4_15.
[26] Luo Y, Akkineni AR, Gelinsky M. Three-dimensional plotting is a versatile rapid prototyping method for the customized manufacturing of complex scaffolds and tissue engineering constructs. Zhongguo Xiu Fu Chong Jian Wai Ke Za Zhi 2014;28:279–85. http://dx.doi.org/10.7507/1002-1892.20140064.
[27] Shim J-H, Lee J-S, Kim JY, Cho D-W. Bioprinting of a mechanically enhanced three-dimensional dual cell-laden construct for osteochondral tissue engineering using a multi-head tissue/organ building system. J Micromech Microeng 2012;22:085014. http://dx.doi.org/10.1088/0960-1317/22/8/085014.
[28] Wang X-Y, Jin Z-H, Gan B-W, Lv S-W, Xie M, Huang W-H. Engineering interconnected 3D vascular networks in hydrogels using molded sodium alginate lattice as the sacrificial template. Lab Chip 2014;14:2709–16. http://dx.doi.org/10.1039/C4LC00069B.
[29] Yao Y, Wei H, Wang J, Lu H, Leng J, Hui D. Fabrication of hybrid membrane of electrospun polycaprolactone and polyethylene oxide with shape memory property. Compos Part B Eng 2015;83:264–9. http://dx.doi.org/10.1016/j.compositesb.2015.08.060.
[30] Doppalapudi S, Jain A, Khan W, Domb AJ. Biodegradable polymers-an overview. Polym Adv Technol 2014;25:427–35. http://dx.doi.org/10.1002/pat.3305.
[31] Sarazin P, Li G, Orts WJ, Favis BD. Binary and ternary blends of polylactide, polycaprolactone and thermoplastic starch. Polymer (Guildf) 2008;49:599–609.
[32] Song J, Gao H, Zhu G, Cao X, Shi X, Wang Y. The preparation and characterization of polycaprolactone/graphene oxide biocomposite nanofiber scaffolds and their application for directing cell behaviors. Carbon N Y 2015;95:1039–50. http://dx.doi.org/10.1016/j.carbon.2015.09.011.
[33] Hutmacher DW. Scaffolds in tissue engineering bone and cartilage. Biomaterials 2000;21:2529–43. http://dx.doi.org/10.1016/S0142-9612(00)00121-6.
[34] Buzarovska A, Gualandi C, Parrilli A, Scandola M. Effect of TiO2 nanoparticle loading on Poly(l-lactic acid) porous scaffolds fabricated by TIPS. Compos Part B Eng 2015;81:189–95. http://dx.doi.org/10.1016/j.compositesb.2015.07.016.
[35] Maio A, Botta L, Tito AC, Pellegrino L, Daghetta M, Scaffaro R. Statistical study of the influence of CNTs purification and plasma functionalization on the properties of polycarbonate-CNTs nanocomposites. Plasma Process Polym 2014;11:664–77. http://dx.doi.org/10.1002/ppap.201400008.
[36] Lo Re G, Lopresti F, Petrucci G, Scaffaro R. A facile method to determine pore size distribution in porous scaffold by using image processing. Micron 2015;76:37–45. http://dx.doi.org/10.1016/j.micron.2015.05.001.
[37] Scaffaro R, Lopresti F, Sutera A, Botta L, Fontana RM, Puglia AM, et al. Effect of PCL/PEG-based membranes on actinorhodin production in streptomyces coelicolor cultivations. Macromol Biosci 2016. http://dx.doi.org/10.1002/mabi.201500391. In Press.
[38] Şengül B, Dilsiz N. Barrier properties of polylactic acid/layered silicate nanocomposites for food contact applications. Polym Sci Ser A 2014;56:896–906. http://dx.doi.org/10.1134/S0965545X14060194.